Seasonality of surface stirring by geostrophic flows in the Bay of Bengal

Nihar Paul

Center for Atmospheric and Oceanic Sciences, Indian Institute of Science, Bangalore

nihar@iisc.ac.in

May 4, 2020

Outline

1. Motivation
2. Introduction and Objectives
3. Finite Time Lyapunov Exponent
4. Finite Size Lyapunov Exponent
5. Data sets and Methods
6. Physical and spectral space characterization
7. Statistical measure of stirring
8. Finite size diffusion coefficient
9. Relative dispersion
10. Conclusion


Gulf of Mexico

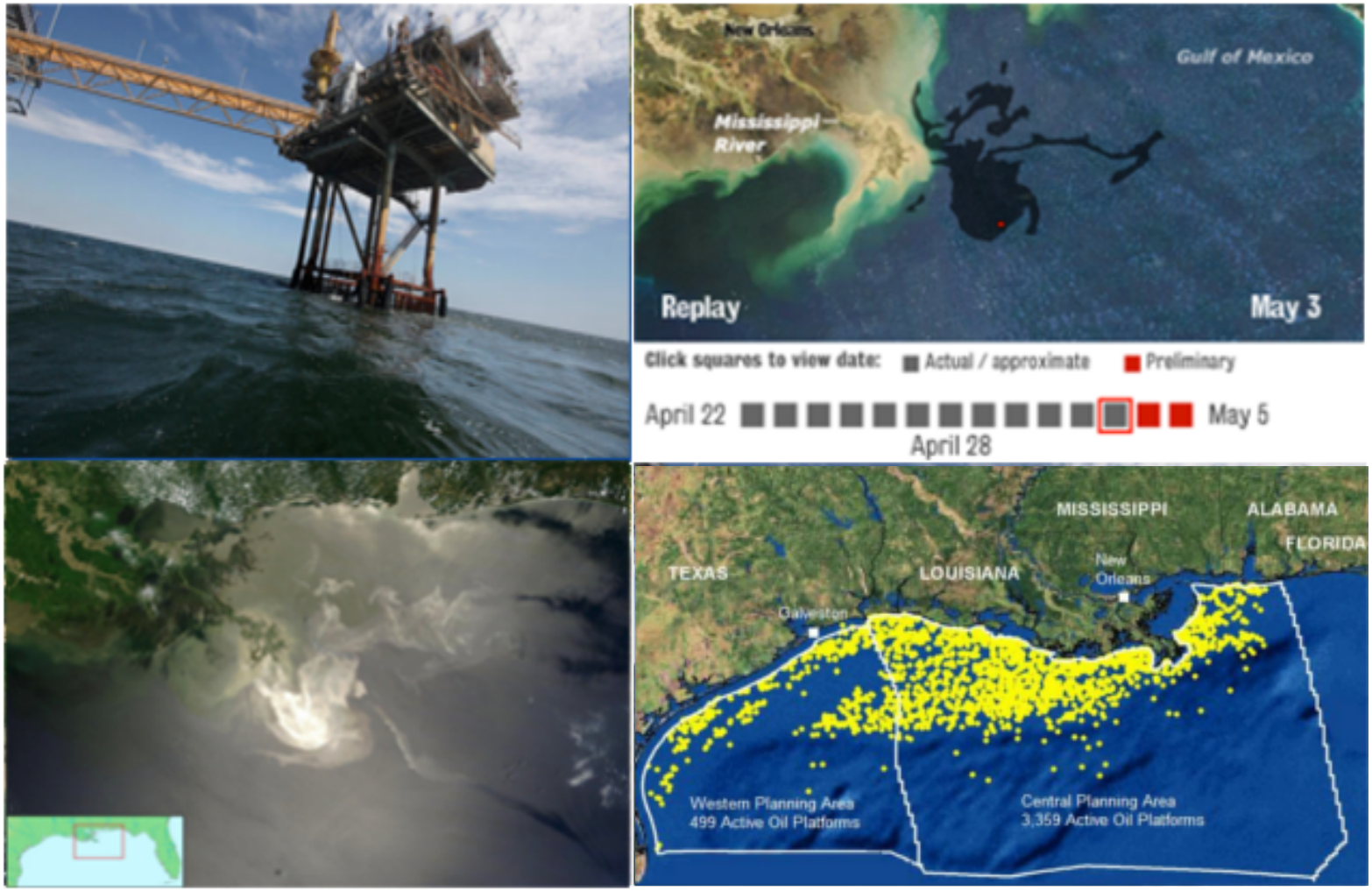

Figure 1: Oil Spill on 24th May, 2010 from MODIS (Moderate-Resolution Imaging Spectroradiometer), Courtesy : NASA, [Mezić et al., 2010], [D'Asaro et al., 2018]

(a)
Red Tide

(b)
Phytoplankton Bloom

(c) ?? --> Salinity

Figure 2: (a) Red algal bloom at Leigh, near Cape Rodney (b) Phytoplankton bloom in Gulf of Aden (c) ?? $--\rangle$ Salinity in Bay of Bengal.

GBM and Irrawaddy Discharge

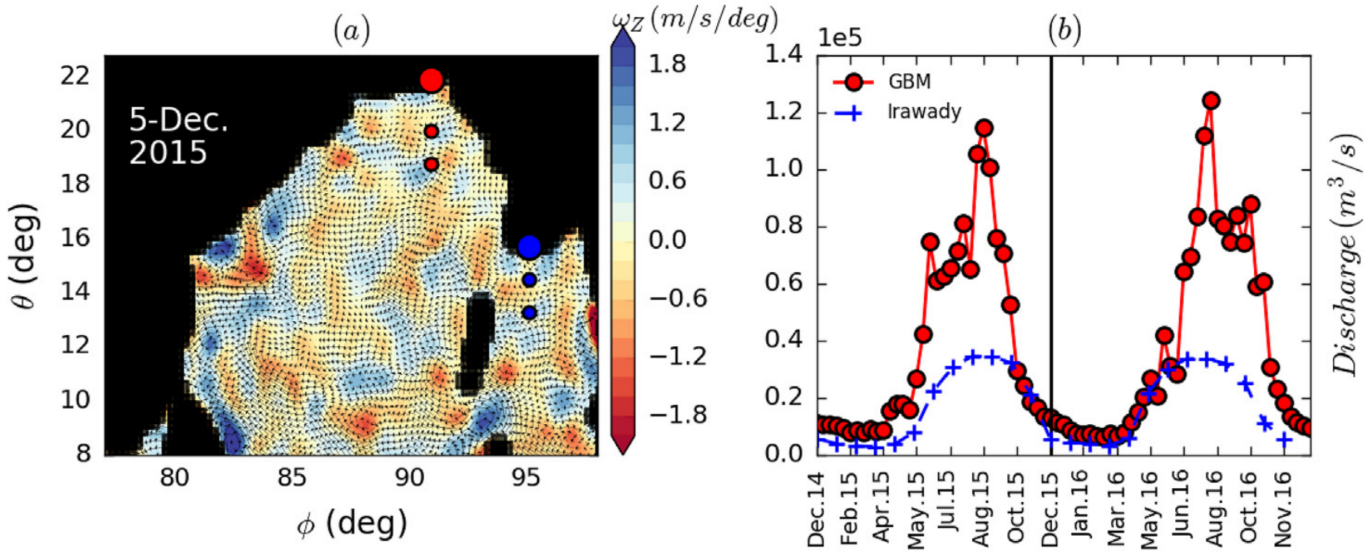

Figure 3: Panel (a) Vorticity field obtained from the satellite-derived currents in the Bay of Bengal on 5 Dec. 2015 with quivers overlaid. The river mouth regions of Ganga-Brahmaputra-Meghna (GBM, red circle at $21.9^\circ N$, $90.90^\circ E$) and Irrawaddy (blue circle at $15.75^\circ N$, $95.07^\circ E$) are also shown. (b) Freshwater discharge from the GBM (red) and Irrawaddy (blue) river mouths during Dec. 2014 to Dec. 2016, plotted every 10 days. The black vertical line indicates 5 Dec. 2015, at which we assume the freshwater discharge for the year 2015 is nearly complete.

[Mathur et al., 2019]

Introduction and Objectives

- To study stirring of **passive scalars** in a **two dimensional non-autonomous** velocity field in the surface of **Bay of Bengal**.
- To present the dynamics of surface geostrophic flow in the **Bay of Bengal**.
- To introduce and explore measures from the theory of dynamical system such as the **Finite Time Lyapunov Exponent (FTLE), Finite Size Lyapunov Exponent (FSLE)** and finally **Relative Dispersion** to characterize the surface geostrophic flow.

Finite Time Lyapunov Exponent

- Lyapunov exponent, this is defined as the exponential rate of separation, averaged over infinite time, of fluid parcels with an initial infinitesimal separation [Benettin et al., 1980].

$$\lambda_\tau(\boldsymbol{x_0}) = \frac{1}{|t - t_0|} \log \frac{\|\delta \boldsymbol{x}(t)\|}{\|\delta \boldsymbol{x}(t_0)\|}. \tag{1}$$

  where, τ is defined as $t - t_0$.

- For non-autonomous flows, the FTLE is essentially a measure of integrated strain along a parcel's trajectory. We calculate the right Cauchy-Green Lagrange tensor $C_{t_0}^t(\boldsymbol{x_0})$ associated with the flow map $F_{t_0}^t(\boldsymbol{x_0})$, which is defined as,

$$C_{t_0}^t(\boldsymbol{x_0}) = \left(\nabla F_{t_0}^t(\boldsymbol{x_0})\right)^T \nabla F_{t_0}^t(\boldsymbol{x_0}). \tag{2}$$

- $F_{t_0}^t(\boldsymbol{x_0})$ denotes the position of a parcel at time t, advected by the flow from an initial time and position $(t_0, \boldsymbol{x_0})$.

- $C_{t_0}^{t}(\boldsymbol{x_0})$ is symmetric and positive definite, its eigenvalues ($\lambda's$) and eigenvectors ($\xi's$) can be written as,

$$C_{t_0}^{t}(\boldsymbol{x_0}) = \lambda_i \xi_i,\ 0 < \lambda_1 \leq \lambda_2, i = 1, 2; \tag{3}$$

$$\nabla F_{t_0}^{t}(\boldsymbol{x_0}) \approx \begin{pmatrix} \alpha_{11} & \alpha_{12} \\ \alpha_{21} & \alpha_{22} \end{pmatrix}, \tag{4}$$

where,

$$\alpha_{i,j} \equiv \frac{x_i(t; t_0, x_0 + \delta x_j) - x_i(t; t_0, x_0 - \delta x_j)}{2|\delta x_j|}. \tag{5}$$


Finite Size Lyapunov Exponent

$$\Lambda(\boldsymbol{x_0}, \delta_0, r) = \frac{\log r}{\tau(\boldsymbol{x_0}; \delta_0, r)}. \tag{6}$$

- This is similar to Equation 1, but here time τ is calculated for a trajectory at a distance δ_0 from a reference trajectory at $\boldsymbol{x}_0$ to reach a separation of distance $r\delta_0$, r being defined as the growth factor [d'Ovidio et al., 2004],[Lehahn et al., 2007].
- Following [García-Olivares et al., 2007], we have also computed the mean FSLE ($\langle\Lambda\rangle$), where a set of N tracers with random initial distribution having standard deviation σ are followed in time as they are transported by the velocity field.

- Defining $\sigma(t)$ as,

$$\sigma(t) = \langle |\boldsymbol{x_i}(t) - \langle \boldsymbol{x_i}(t) \rangle|^2 \rangle^{1/2}, \tag{7}$$

where,

$$\langle \boldsymbol{x_i}(t) \rangle \equiv \langle \{\boldsymbol{x_i}(t) : i = 1, 2, ...N\} \rangle = \frac{1}{N} \sum_{i=1}^{N} \boldsymbol{x_i}(t). \tag{8}$$

- We set the initial size of the cluster σ_0 according to Equations 7 and 8, and measure the time $\tau(\boldsymbol{x_0};\ \sigma_0,\ r)$ as it takes the growth from σ_0 to $\sigma_f = r\sigma_0$ where r is the growth factor and σ_f being the largest scale under consideration (the sub-basin scale). The mean FSLE parameter as a function of the scale is then obtained from,

$$\langle \Lambda(\boldsymbol{x_0},\ \sigma_0,\ r) \rangle = \frac{\log r}{\tau(\boldsymbol{x_0},\ \sigma_0,\ r)}, \tag{9}$$

which is not sensitive when variation in r is close to $1+$.

Data sets

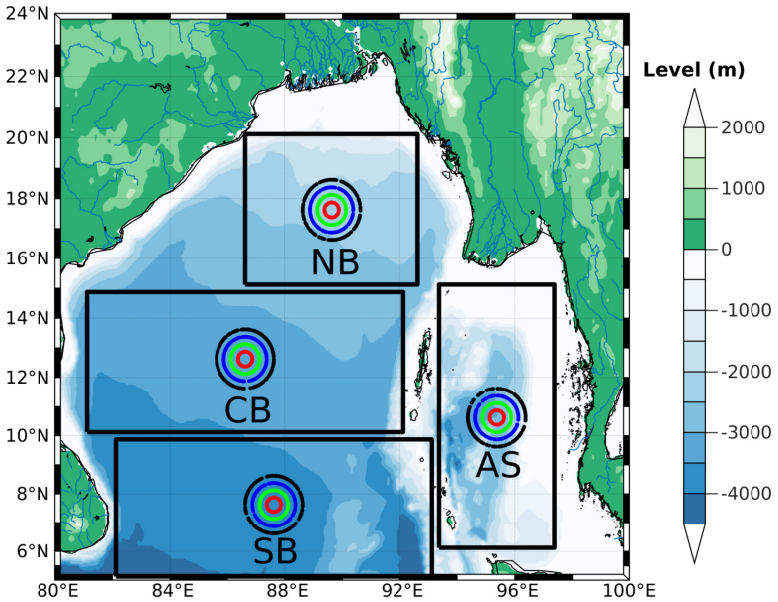

Figure 4: Bay of Bengal

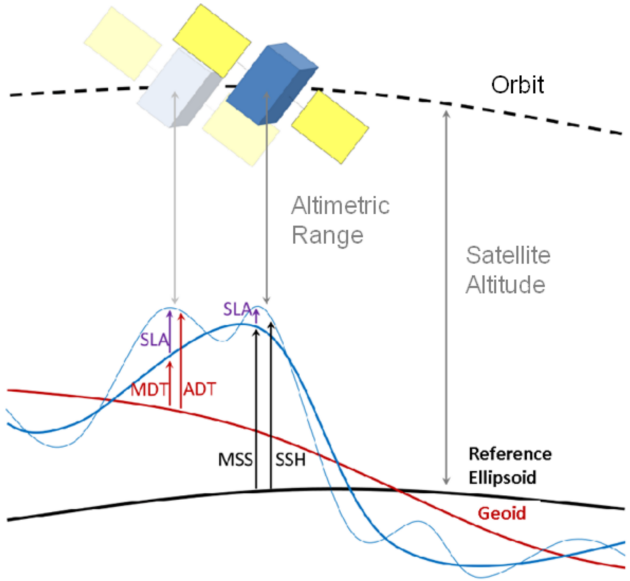

Figure 5: Altimetric Principle

- **MADT-H-UV** data from 2008-2017 have been used.
- Spatial resolution is **0.25**°x**0.25**°.
- For advection we have used RK4 method along with bilinear interpolation of velocity field across the grid.

Physical space characterization

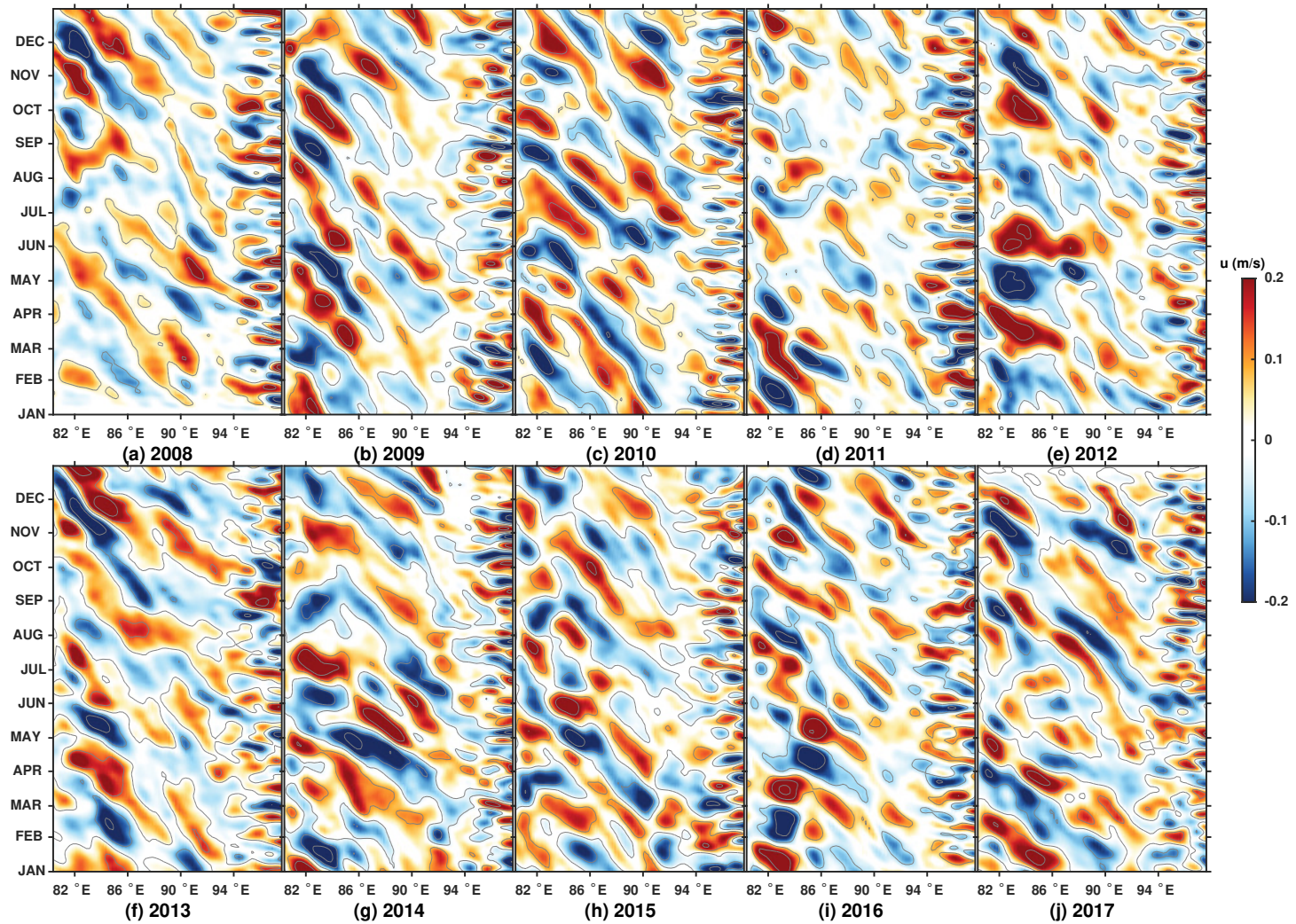

Figure 6: Panels (a)-(j) show Hovmöller diagrams of the filtered 10-120 day zonal geostrophic velocity from 2008 to 2017, respectively. The plots are averaged over 14.125°N-15.125°N from a longitude of 80.375°E to 97.625°E in the BoB.

Spectral space characterization

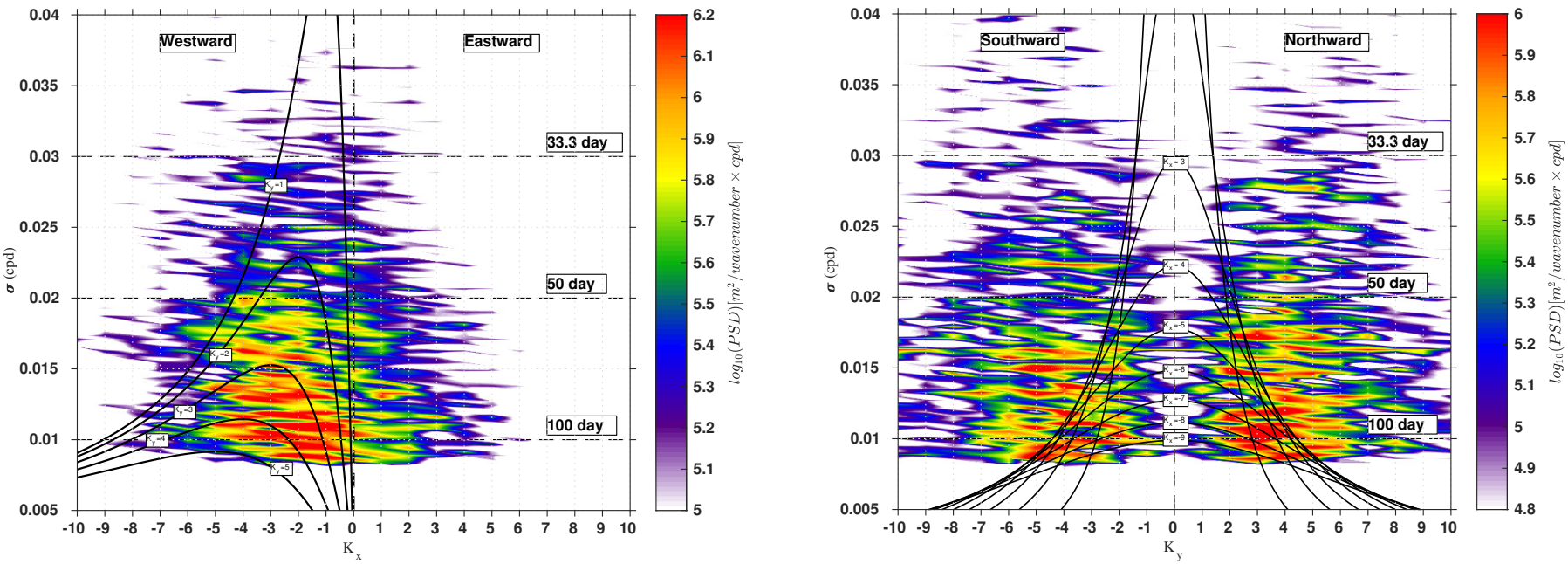

(a) **(b)**

Figure 7: Wavenumber-frequency plots of 10-120 day filtered zonal geostrophic velocity. Panels (a) and (b) show $\sigma - K_x$, averaged over 14.125°N-15.125°N and $\sigma - K_y$, averaged over 89.625°E-90.625°E, respectively. Solid black lines are theoretical linear Rossby wave dispersion curves.

Spectral space characterization

$$\sigma = -\frac{\beta k_x}{{k_x}^2 + {k_y}^2 + \frac{1}{L_R^2}}, \text{for } k_x, k_y = 1, 2, 3.... \tag{10}$$

- Here, k_x and k_y are the zonal and meridional wavenumber and $L_R = NH/\sqrt{n\pi fo}$ is the Rossby radius of deformation. The wavenumbers have been normalized by the length of the BoB which is equal to 1870 km at 14.125°-15.125°N.
- The typical value of L_R, lies between 60-140 km over the latitudes spanned by the Bay [Chelton et al., 1998].
- In fact, following [Stammer, 1997], we estimated an "eddy length scale" from zero crossing of autocorrelation function of the SSH. This estimate (not shown) is larger than L_R [Chen et al., 2012], and varies approximately from 55-200 km over 22°N and 6°N.

Spectral space characterization

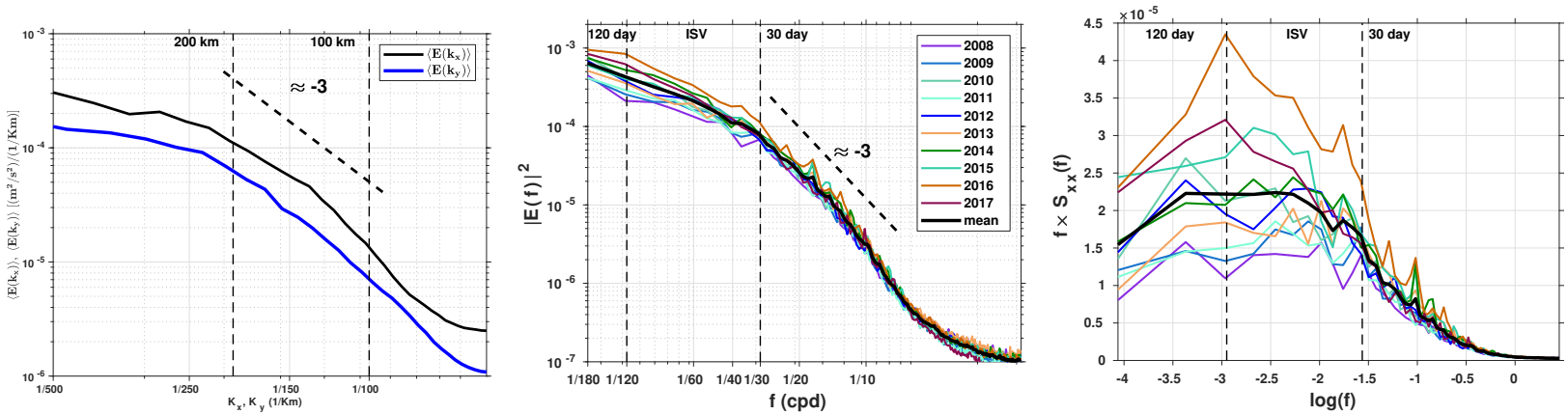

Figure 8: Kinetic energy spectra. Panel (a) shows zonal and meridional wavenumber spectra averaged over 11.125°N-12.125°N and 89.625°E-90.625°E, respectively (through the widest longitudinal and latitudinal extent of the Central Bay). Panels (b) and (c) contain temporal spectra vs f (frequency) in log-log scale and variance preserving form, respectively. Spectra are estimated at each grid point and then averaged for a year.

A Sign of chaos

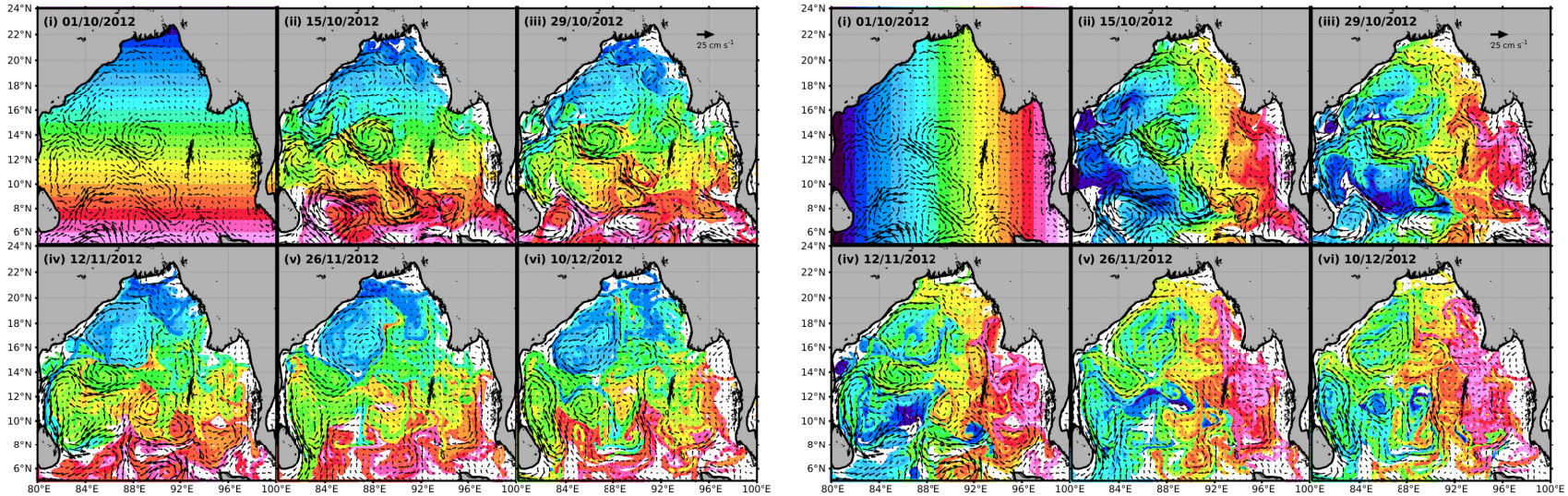

Figure 9: The stirring of latitudinal (first six panels) and longitudinal (last six panels) bands by geostrophic currents from October to December 2012. Snapshots are shown every two weeks for ten week long advection.

Finite time and Finite Size Lyapunov Exponents

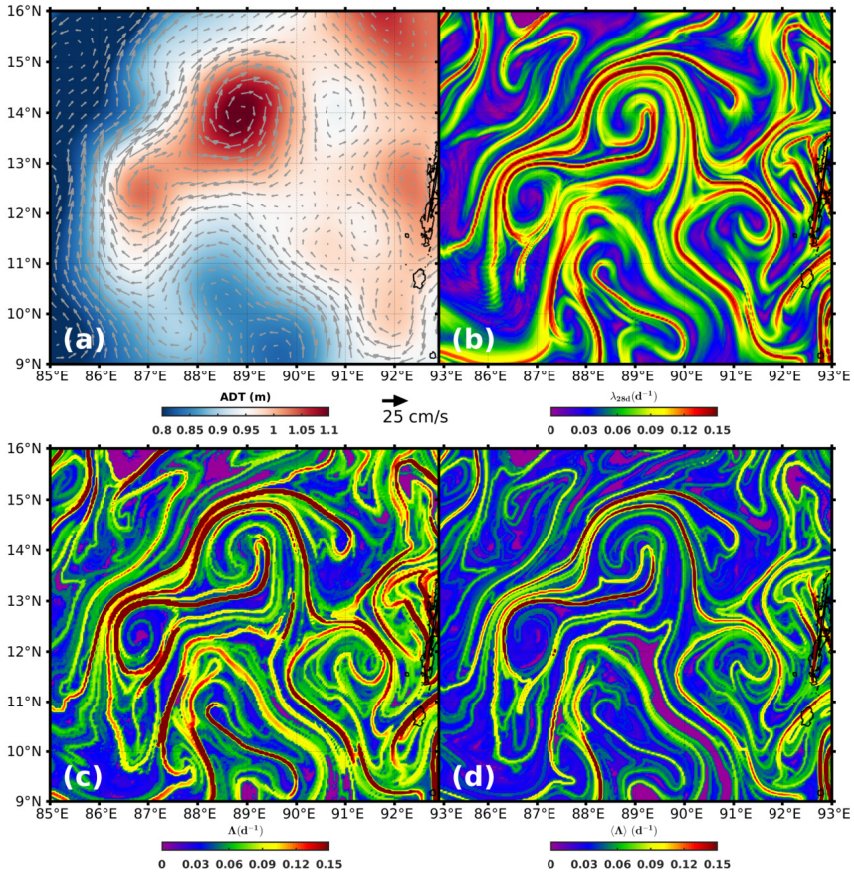

Figure 10: Panels (a), (b), (c) and (d) show absolute dynamic topography (with geostrophic quivers), FTLE- 28 days (λ_{28d}), FSLE (Λ) and mean FSLE ($\langle\Lambda\rangle$) computed on $\frac{1}{32}^\circ \times \frac{1}{32}^\circ$ grid resolution starting from 18/10/2009. The growth factor r for FSLE (Λ, $\langle\Lambda\rangle$) computation was taken as 32 i.e. δ_0 (σ_0) and δ_f (σ_f) are $\frac{1}{32}^\circ$ and 1°, respectively.

Finite time and Finite Size Lyapunov Exponents

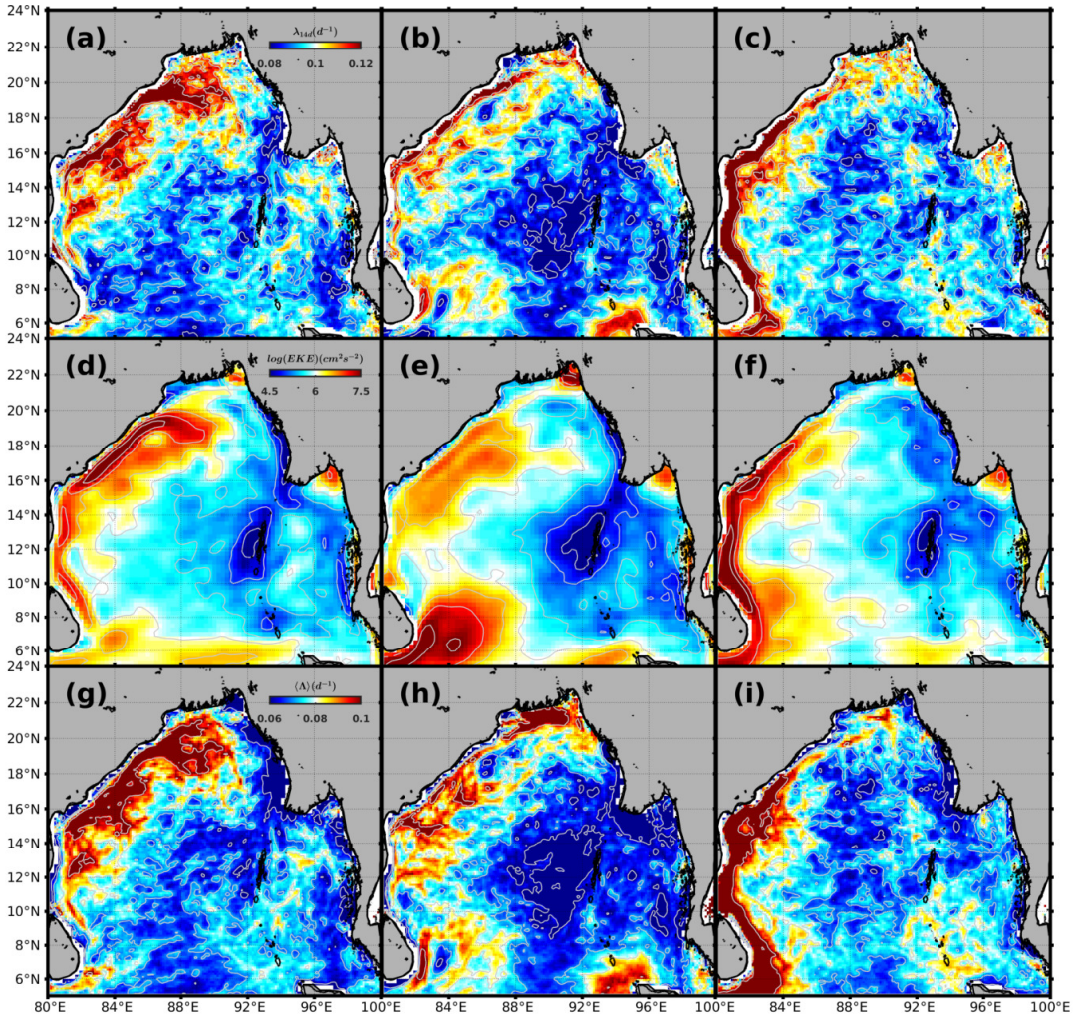

Figure 11: Panels (a) and (d) show the seasonal mean FTLE-14 days (λ_{14d}) and EKE maps for FMA, (b) and (e) for JJAS, (c) and (f) for the OND seasons, respectively. Panels (g), (h) and (i) show the corresponding seasonal mean FSLE ($\langle\Lambda\rangle$) maps for FMA, JJAS and OND seasons, respectively.

Statistical measure of stirring

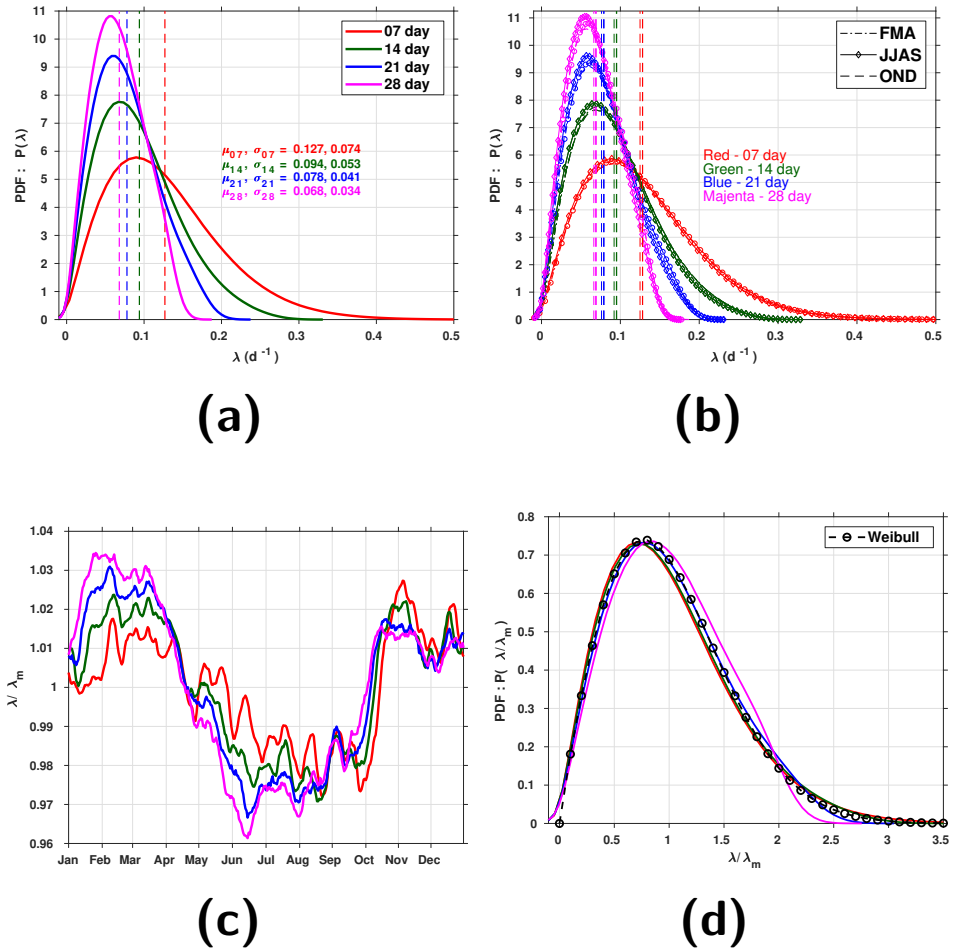

Figure 12: Histogram of FTLEs (with different increments) over the Bay; (a) whole year (b) in different seasons. Panel (c) shows the daily time series of mean FTLE (normalized by mean λ of all the ten years) through the year. Panel (d) shows a fit to the FTLE distributions (normalized by mean λ) for different τ by a Weibull distribution.

Statistical measure of stirring

- We note that a Weibull distribution accurately fits the FTLE histogram normalized by the mean FTLE.

$$P_W(\lambda) = \frac{b}{a}\left(\frac{\lambda}{a}\right)^{b-1} \exp\left(-\frac{\lambda^b}{a^b}\right), \tag{11}$$

- The value of $a = 1.13$ and $b = 1.92$.

Finite Size Diffusion Exponent

- **FSDC** is abbreviated as **Finite Size Diffusion Coefficient**.
- It can be expressed by following **dimensional** analysis :

$$D(\sigma) = \sigma^2 \langle \Lambda \rangle (\sigma). \tag{12}$$

- As the cluster size grows, if it is driven by chaos at very small scales ($\ll l_u$) and by (eddy) diffusion at very large scales ($\gg l_u$), then $\langle \Lambda \rangle (\sigma)$ has the following asymptotic behavior,

$$\langle \Lambda \rangle (\sigma) = \begin{cases} \langle \Lambda \rangle_{max}, & \text{if } \sigma \ll l_u, \\ \frac{D}{\sigma^2}, & \text{if } \sigma \gg l_u. \end{cases} \tag{13}$$

[García-Olivares et al., 2007]

Finite size diffusion coefficient

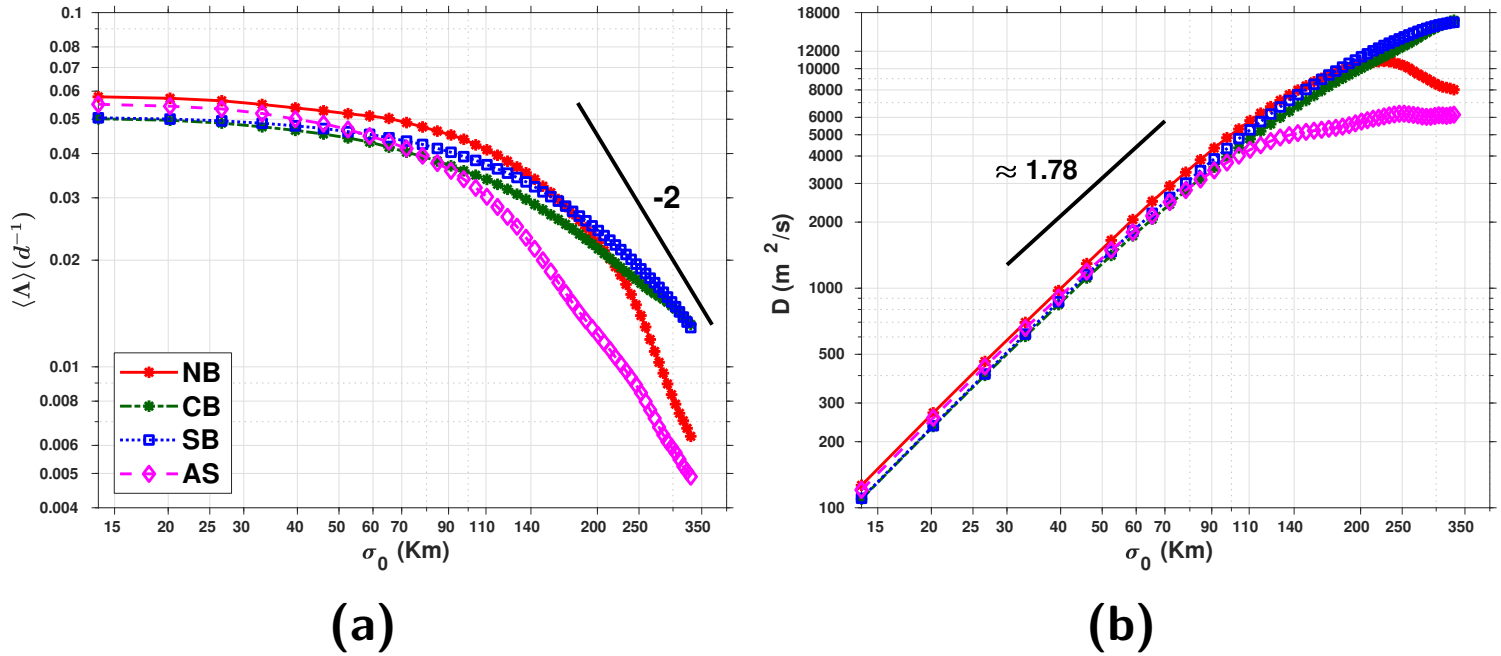

Figure 13: Panels (a) and (b) show FSLE and eddy diffusivity as a function of initial standard deviation with expansion factor $r = 1.2$ for the Northern Bay, Central Bay, Southern Bay and Andaman Sea.

Relative Dispersion

- $\langle R^2(t) \rangle$ is the mean relative dispersion of an ensemble of N pairs having the same initial separation with random orientation.

$$\langle R^2(t) \rangle = \frac{1}{N(N-1)} \sum_{i \neq j} {R^2}_{ij}(t) \tag{14}$$

[Waugh and Abraham, 2008];[Poje et al., 2017];[LaCasce, 2010]

Relative dispersion

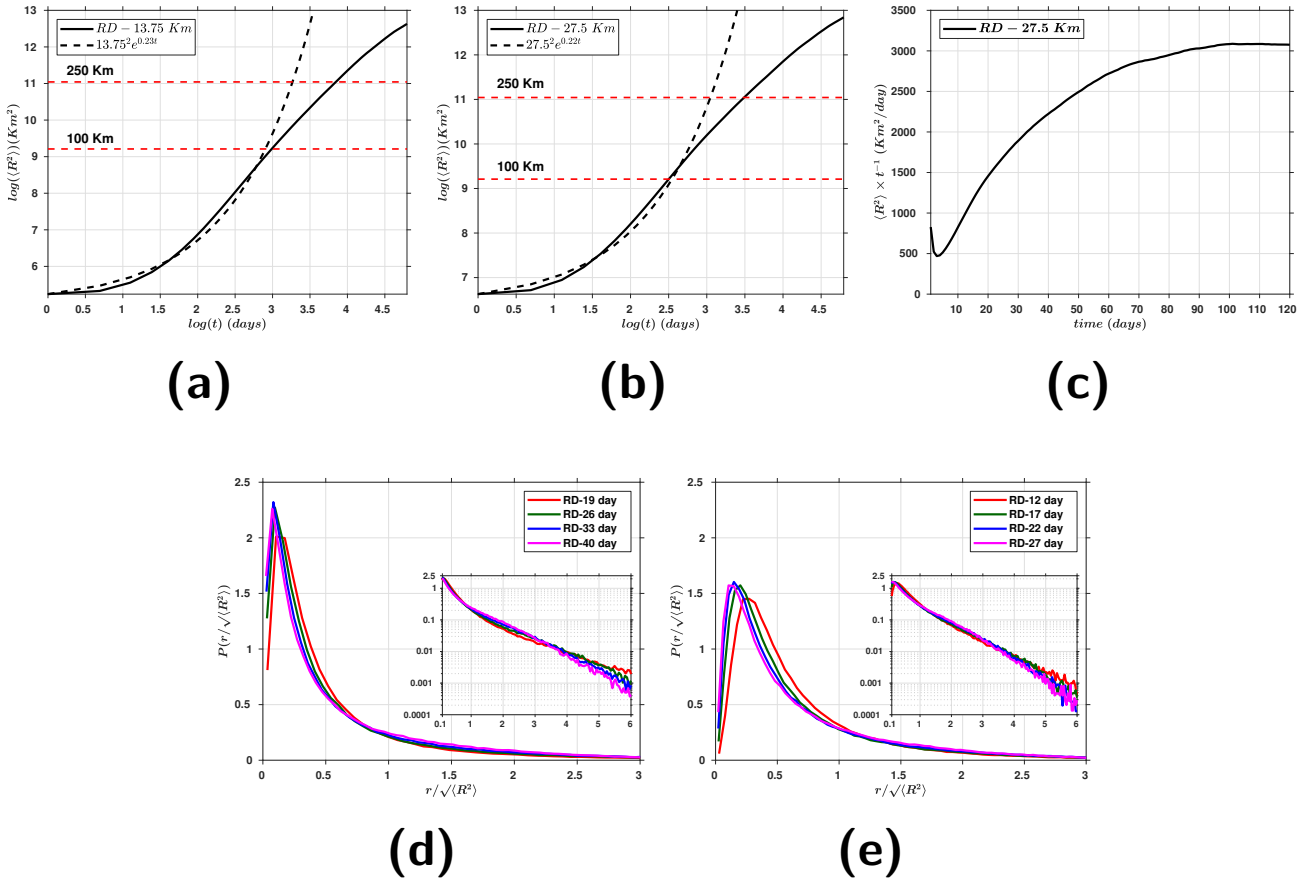

Figure 14: Panels (a) and (b) show the RD with time for initial separations of 13.75 and 27.5 km, respectively. Panel (c) shows the compensated RD (by t^{-1}) as a function of time for the initial separation of 27.5 km. Panels (d) and (e) show histograms of the square root of RD (denoted by r, normalized by its rms value) at different days when the mean RD is between 100 and 250 km.

Thermal Front

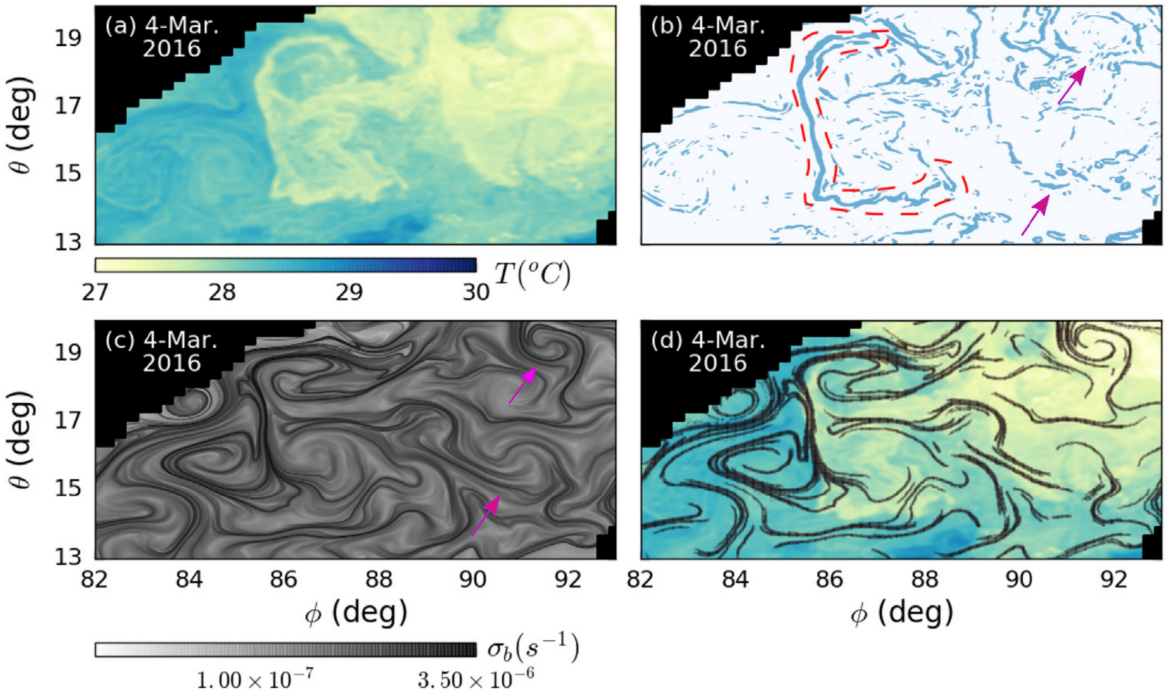

Figure 15: (a) Spatial distribution of sea surface temperature (SST) on 4 Mar.2016, (b) Points (shown in blue) that satisfy $|\nabla(\text{SST})| > 0.02°/\text{km}$ on 4 Mar.2016, (c) the bFTLE field σ_b (computed using $T_I = 20$ days) on 4 Mar.2016, and (d) points (shown in black) that satisfy $\sigma_b > 0.5\sigma_{bmax}$ plotted on top of the SST distribution on 4 Mar.2016. The red dashed line in (b) encompasses the C-front region. The pink arrows in (b) and (c) show other prominent features that are similar between the $|\nabla(\text{SST})|$ and bFTLE fields.

[Mathur et al., 2019]

Conclusion

- We examined the flow by means of Hovmöller plots and wavenumber-frequency diagrams. It was seen that the geostrophic currents in the Bay are dominated by westward progressing disturbances that have temporal scales between 50 and 120 days.
- The power in these systems aligned well with the theoretical dispersion curves for linear baroclinic Rossby waves. Interestingly, some of these have length scales that are smaller than the local deformation scale, and show an eastward group velocity which was noted in the Hovmöller plots.
- Temporal and spatial power spectra were seen to follow approximate power-laws (-3 scaling, from 100-250 km and 10-30 days, respectively) and suggested an uninterrupted distribution of power across these length and subseasonal time scales.

Conclusion

- Maps of the FTLEs and FSLEs suggested an equatorward movement of regions of enhanced stirring from pre-monsoonal to post-monsoonal periods.
- In each season, stirring along the coasts is vigorous while the central Bay had relatively low FTLE values, suggestive of the presence of kinematic barriers that were consistent with the eddy scale of stirring noted above. The low stirring rates in the central Bay are especially stark in the monsoon season.
- Specific seasonal features, such as enhanced stirring at the mouth of GBM, the appearance of the Sri Lankan dome in the monsoon and the BoB dome in winter, were captured by high FTLE and mean FSLE pockets. Also, overall, the spatial maps of seasonal mean FTLE and mean FSLE were in tune with those of EKE, with high EKE aligned with regions of rapid stirring.


Conclusion

- The non-uniform nature of surface stirring in the Bay was manifested in probability density functions of FTLEs that had long tails and their shape, and as in other parts of the world's oceans, was captured by a Weibull distribution.
- In terms of a domain average, the FTLE for a week's increment was approximately 0.13 day^{-1}, while the spread captured by the histogram ranged up to 0.6 day^{-1}.
- In addition, with longer time increments, the distribution of FTLEs became taller (and smaller mean), but with progressively more stretched exponential with lighter tails. Thus, the non-uniformity of mixing was further highlighted at longer time intervals.
- This quantitative estimate of the distribution of FTLEs is potentially useful in developing kinematic models, such as for the dispersal of pollutants in the Bay.


Conclusion

- Below 100 km, the smoothly interpolated nature of the data results in pair separation that was exponential in time.
- From 100 to 250 km, i.e. the RD followed a power-law in time, which is consistent a forward enstrophy transfer regime, but with a variable enstrophy flux.
- At larger scales, the pair separation took on an eddy-diffusive growth, i.e. $\langle R^2 \rangle \sim t$, with a diffusivity of the order of 10^4 $m^2 s^{-1}$ when averaged over the BoB.
- Averaging the growth of clusters for all days across 10 years, the mean FSLE was relatively constant (up to 100 km), transitions (from 100 to 250 km) and then enters an eddy-diffusive regime (from 250-300 km).
- The Andaman Sea was seen to enter an eddy-diffusive regime at relatively smaller scales (between 140-200 km) while the central Bay showed no signs of this transition.

Conclusion

- The large scale eddy-diffusivity, with each eddy acting independently and inducing a random walk, estimated from the mean FSLE plots was about 1.6×10^4 $m^2 s^{-1}$ in the Southern Bay, 8×10^3 $m^2 s^{-1}$ in the Northern Bay and approximately 6×10^3 $m^2 s^{-1}$ in the Andaman Sea region.
- Interestingly, before the emergence of an eddy-diffusive regime, the finite size diffusion coefficient showed a similar power-law behavior in all regions of the Bay (exponent of 1.78 with cluster size).


Abernathey, R. and Marshall, J. (2013).
Global surface eddy diffusivities derived from satellite altimetry.
Journal of Geophysical Research, 118:901–916.


Benettin, G., Galgani, L., Giorgilli, A., and Strelcyn, J.-M. (1980).
Lyapunov characteristic exponents for smooth dynamical systems and for Hamiltonian systems; a method for computing all of them. Part 1: Theory.
Meccanica, 15(1):9–20.


Chelton, D. B., Deszoeke, R. A., Schlax, M. G., El Naggar, K., and Siwertz, N. (1998).
Geographical variability of the first baroclinic rossby radius of deformation.
Journal of Physical Oceanography, 28(3):433–460.


Chen, G., Wang, D., and Hou, Y. (2012).
The features and interannual variability mechanism of mesoscale eddies in the Bay of Bengal.
Continental Shelf Research, 47:178–185.

Corrado, R., Lacorata, G., Palatella, L., Santoleri, R., and Zambianchi, E. (2017).
General characteristics of relative dispersion in the ocean.
Scientific Reports, 7:46291.

D'Asaro, E. A., Shcherbina, A. Y., Klymak, J. M., Molemaker, J., Novelli, G., Guigand, C. M., Haza, A. C., Haus, B. K., Ryan, E. H., Jacobs, G. A., et al. (2018).
Ocean convergence and the dispersion of flotsam.
Proceedings of the National Academy of Sciences, 115(6):1162–1167.

d'Ovidio, F., Fernández, V., Hernández-García, E., and López, C. (2004).
Mixing structures in the mediterranean sea from finite-size lyapunov exponents.
Geophysical Research Letters, 31(17).

García-Olivares, A., Isern-Fontanet, J., and García-Ladona, E. (2007).
Dispersion of passive tracers and finite-scale Lyapunov exponents in the Western Mediterranean Sea.

Deep Sea Research Part I: Oceanographic Research Papers, 54(2):253–268.


Khatri, H., Sukhatme, J., Kumar, A., and Verma, M. (2018).
Surface ocean enstrophy, kinetic energy fluxes and spectra from satellite altimetry.
Journal of Geophysical Research.


LaCasce, J. (2010).
Relative displacement probability distribution functions from balloons and drifters.
Journal of Marine Research, 68:433–457.


Lehahn, Y., d'Ovidio, F., Lévy, M., and Heifetz, E. (2007).
Stirring of the northeast atlantic spring bloom: A lagrangian analysis based on multisatellite data.
Journal of Geophysical Research: Oceans, 112(C8).


Lin, J. (1972).
Relative dispersion in the enstrophy cascading inertial range of homogeneous two-dimensional turbulence.


Journal of the Atmospheric Sciences, 29:394.


Mathur, M., David, M. J., Sharma, R., and Agarwal, N. (2019).
Thermal fronts and attracting lagrangian coherent structures in the north bay of bengal during december 2015–march 2016.
Deep Sea Research Part II: Topical Studies in Oceanography, 168:104636.


Mezić, I., Loire, S., Fonoberov, V. A., and Hogan, P. (2010).
A new mixing diagnostic and gulf oil spill movement.
Science, 330(6003):486–489.


Poje, A. et al. (2017).
Evidence of a forward energy cascade and Kolmogorov self-similarity in submesoscale ocean surface drifter observations.
Physics of Fluids, 29:020701.


Stammer, D. (1997).
Global characteristics of ocean variability estimated from regional topex/poseidon altimeter measurements.
Journal of Physical Oceanography, 27(8):1743–1769.



Waugh, D. W. and Abraham, E. R. (2008).
Stirring in the global surface ocean.
Geophysical Research Letters, 35(20).


Publication

1. Nihar Paul, Jai Sukhatme, *Deep-Sea Research II, https://doi.org/10.1016/j.dsr2.2019.104864*.

Question ?

Additional Slides : 1

Estimation of Eddy diffuisivity

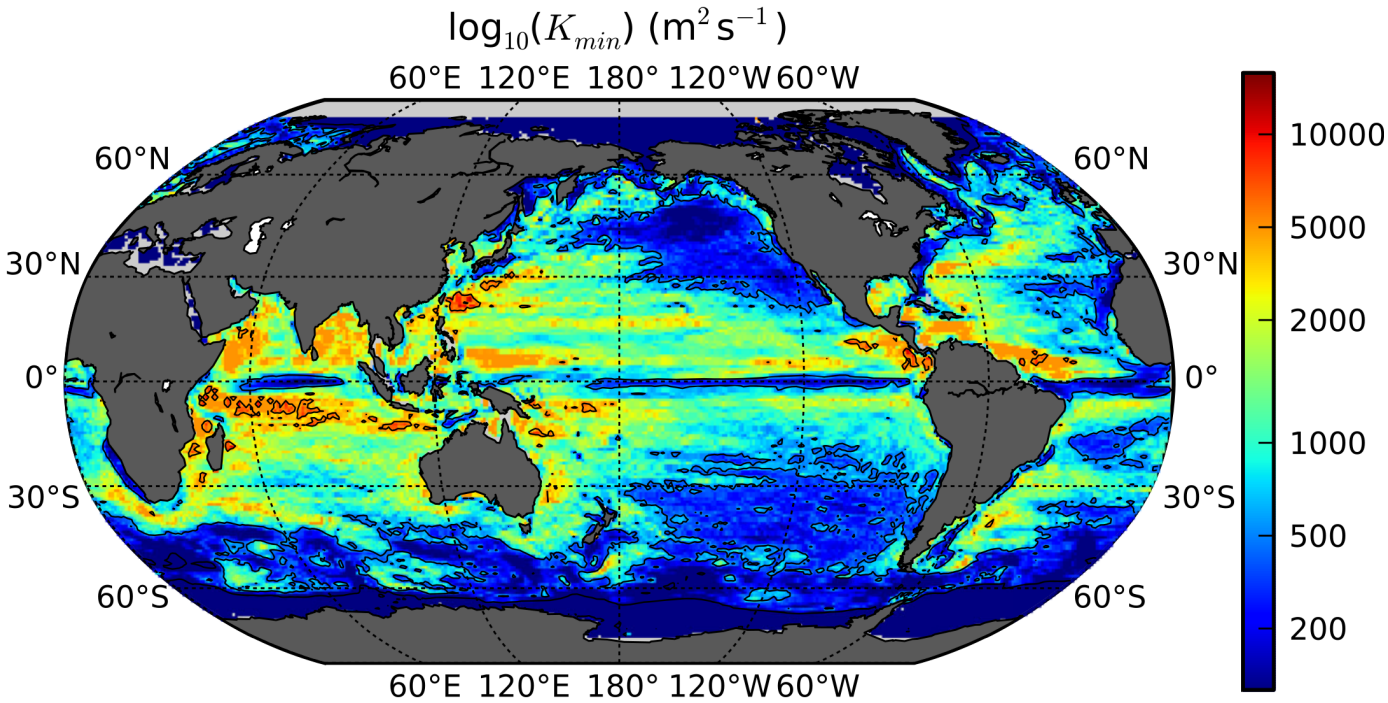

Figure 16: Composite value of K produced by taking the minimum K_{OC} at each point from the three experiments.

[Abernathey and Marshall, 2013]

Additional Slides : 2

Estimation of Eddy diffuisivity from FSLEs across global ocean

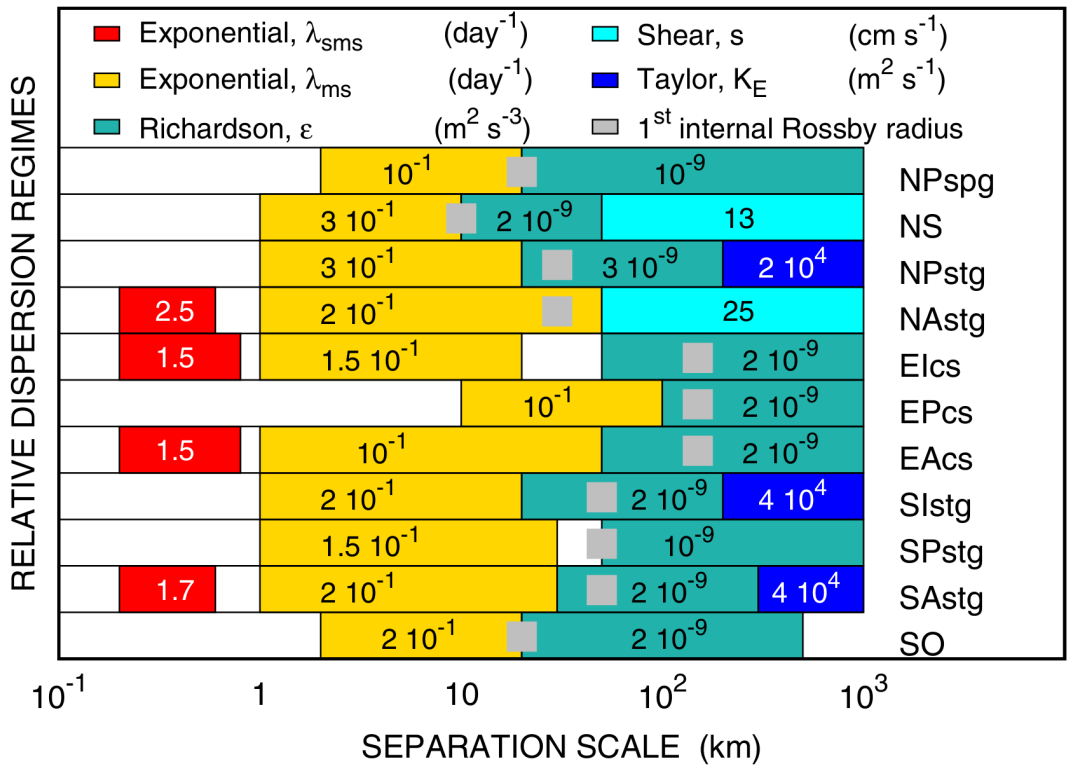

Figure 17: Composite value of K produced by taking the minimum K_{OC} at each point from the three experiments.

[Corrado et al., 2017]

Additional Slides : 3

Derivation of relative dispersion in the enstrophy-cascading intertial range of homogeneous two-dimensional turbulence

1. Introduction

The well-known Richardson's law (1926) for the dependence of turbulence diffusivity on the relative particle separation $(\overline{\xi_r^2})^{\frac{1}{2}}$ in homogeneous three-dimensional turbulence can be obtained by using dimensional arguments (Obukhov, 1941) provided the relative particle separation is within the energy-cascading inertial range where ϵ, the total dissipation rate, is the essential characteristic parameter. Here, by dimensional arguments, a theory of the relative dispersion in the enstrophy-cascading inertial range of homogeneous two-dimensional turbulence will be derived.

2. Analysis

Through the studies of Kraichnan (1967), Leith (1968) and Batchelor (1969), the enstrophy-cascading range is characterized by an enstrophy (half-squared vorticity) cascade rate η. In this range the characteristic time scale is $\eta^{-\frac{1}{3}}$ and the energy spectrum $E(k)$ has the form $E(k) \propto \eta^{\frac{2}{3}} k^{-3}$, where k is the wavenumber. Now it is postulated that the turbulence diffusivity K, defined by $\frac{1}{2}(d\overline{\xi_r^2}/dt)$, depends on $\overline{\xi_r^2}$ and η only. Hence, by dimensional arguments, we have

$$K = \frac{1}{2}\frac{d\overline{\xi_r^2}}{dt} = A\eta^{\frac{1}{3}}\overline{\xi_r^2}, \qquad (1)$$

where A is a positive constant with the order of unity provided that turbulent mixing is the dominate process for dispersion, and t is the time. Integrating (1) yields

$$\overline{\xi_r^2} = \overline{\xi_{r0}^2}\exp(2A\eta^{\frac{1}{3}}t) \text{ or } 2.3\log(\overline{\xi_r^2}/\overline{\xi_{r0}^2}) = 2A\eta^{\frac{1}{3}}t, \qquad (2)$$

where $\overline{\xi_{r0}^2}$ is the integration constant referenced at $t=0$. Eq. (2) then describes the relative dispersion in the enstrophy-cascading inertial range of homogeneous two-dimensional turbulence.

3. Discussion

Although it is known that the large-scale motions in the atmosphere are quasi-horizontal, a direct application of (2) to the large-scale dispersions in the atmosphere must be justified. Recently, Charney (1971) developed a geostrophic turbulence theory for three-dimensional quasi-geostrophic flow. According to him, the large-scale motions in the atmosphere are similar to geostrophic turbulence rather than to two-dimensional turbulence, i.e., the large-scale motions at high wave-

[1] Present affiliation: Flow Research, Inc., Kent, Washington.
[2] The National Center for Atmospheric Research is sponsored by the National Science Foundation.

Figure 18

[Lin, 1972]

Additional Slides : 4

Enstrophy as a function of scale

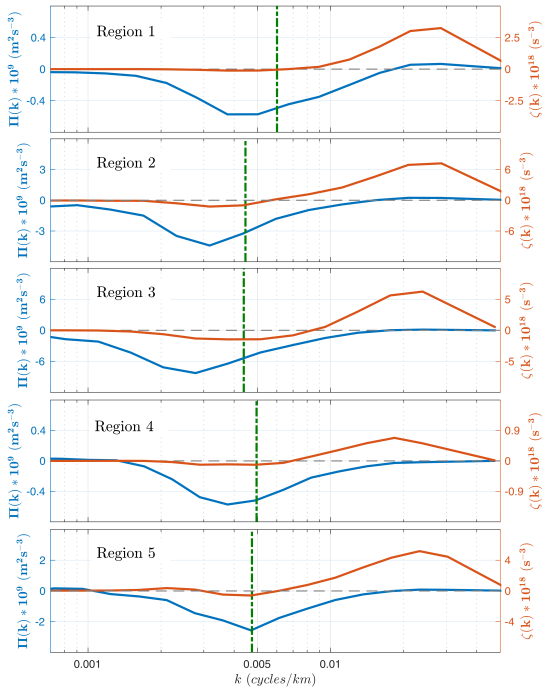

Figure 19: KE ($\Pi(k)$, blue) and enstrophy (ζ, red) fluxes computed using geostrophic currents from POP model data (averaged over 1 year) versus wave number q ($k = \sqrt{k_x^2 + k_y^2}$). Vertical dashed lines mark the transition scale ($\sqrt{\langle KE \rangle / \langle Z \rangle}$) in each region.

[Khatri et al., 2018]